CHAPTER 4 RESULTS AND DISCUSSION

4.1 Diagnostics

4.1-a Introduction

The various aspects of the experiments performed in course of our studies and their results are described in the following sections. They can be grouped into preliminary sample preparation procedures, the actual experiments, and, finally, an analysis of the results.

Preliminary procedures were performed prior to the actual experiments to ensure pure, defect-free sample surfaces and also to determine the onset of Cs saturation of the samples at room temperature. Auger electron spectroscopy (AES) was used to determine the level of surface contaminants of both the clean and the cesium-adsorbed surfaces. Low Energy Electron Diffraction (LEED) images of the surfaces were used to determine the surface structure of the clean surfaces prior to deposition. A series of AES scans were used to plot Auger uptake curves to determine the onset of cesium saturation. The outcome of the various diagnostic probes, are outlined in the following sections.

4.1-b Contaminant levels of the clean Si surfaces:

The clean reconstructed Si crystal surfaces are highly reactive. There are always residual impurities like CO, hydrocarbons compounds and water, adsorbed into the walls of the chamber that keep diffusing slowly even in UHV. These species react with the clean Si surfaces and usually causing C and O contamination over time.

Figure 4.1 shows a typical AES scan from a contaminated or poorly prepared cesium adsorbed sample for illustration purposes. The surface was obtained by dosing Cs from a Cs getter source before it was degassed and cleaned. The sizes of the elemental peaks are an indicator of the types and the levels of impurities, and obviously, the goal is to remove or minimize them. The intensity of the Si peak diminishes with carbon or oxygen impurities because they shield the substrate signal. The ratio of the AES signal intensities compensated for the sensitivities of the Auger transitions at a given beam energy is denoted by:

$$R_{impurity-Si} = \frac{I_{impurity}/S_{impurity}}{I_{Si}/S_{Si}}$$

This metric can be used to compare the impurity levels of different samples and also give an idea of the relative concentrations of different surface elements. For the sample in Figure 4.1, R_{O-Si} is 20 % and R_{C-Si} is 12 % which means that the ratio of Oxygen to Carbon on the surface is approximately 20:12. An estimate of the relative atomic concentrations of the impurities on the surface making use of the AES signal heights and the relative sensitivities of the respective peaks are shown in table Table 4-1.

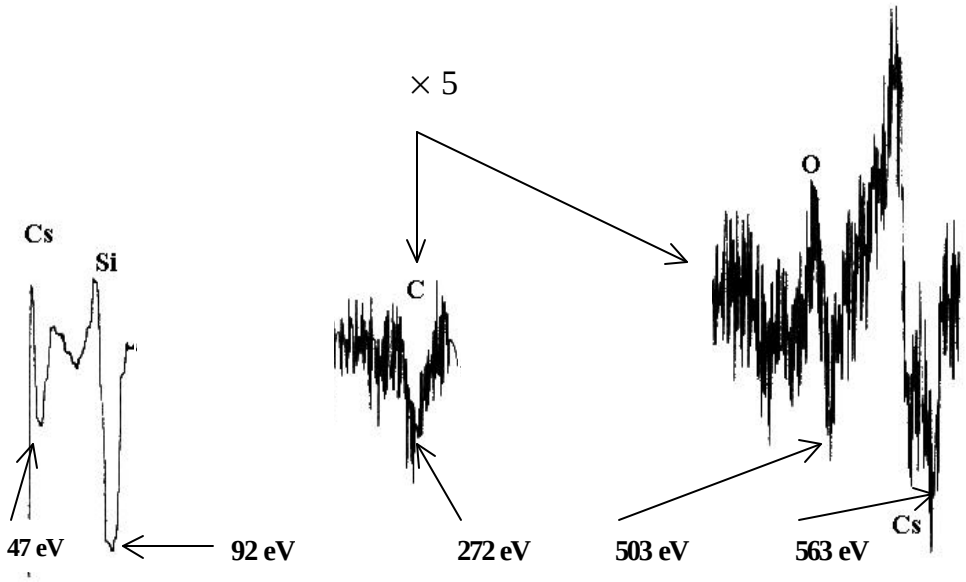

Figure 4.1 Auger spectrum for a poor quality Cs/Si(111) 7×7 interface. The vertical axis is dN/dE, horizontal axis is energy (same for all following spectra). The low energy Cs (47 eV) and Si (92 eV) peaks are scaled down by a factor of 5 relative to the other peaks. (The tall, thin spikes in the C and O peaks are just noise.)

Table 4-1 Contamination levels of the Cs layer based on AES intensities of Figure 4.1.

Element	Peak Energy (eV)	Signal Height (inches)	Sensitivity Factor[6]	Relative Atomic Concentration (signal/sensitivity)	Percentage
C	271	1.2	0.21	6	18%
O	503	2.0	0.52	4	12%
Cs	563	3.7	0.17	22	70%

AES scans of clean surfaces of typical samples used in experiments, for the Si(100) 2×1, Si(111) 7×7 and Si(111)($\sqrt{3}\times\sqrt{3}$)R30°–B surfaces are shown in Figure 4.2, Figure 4.3 and Figure 4.4 respectively. The carbon and oxygen signals from these surfaces are barely detectable or non-existent, whereas for the cesium adsorbed samples in Figure 4.6, Figure 4.7 and Figure 4.8, the ratios($R_{impurity\text{-}Si}$) are just above noise level at ~3-4 %.

The Cs coverage is measured based on the 47 eV peak for Cs, which is the strongest peak for a 3 keV primary electron beam. For purposes of comparison with oxygen and carbon contaminants, it is more convenient to use the peak at 563 eV.

More care needs to be taken during the preparation of the Si(100) surface as compared to the other surfaces because of its greater reactivity as compared to the Si(111) 7×7 surface, and consequently a large number of trials to identify a proper procedure for surface preparation were needed.

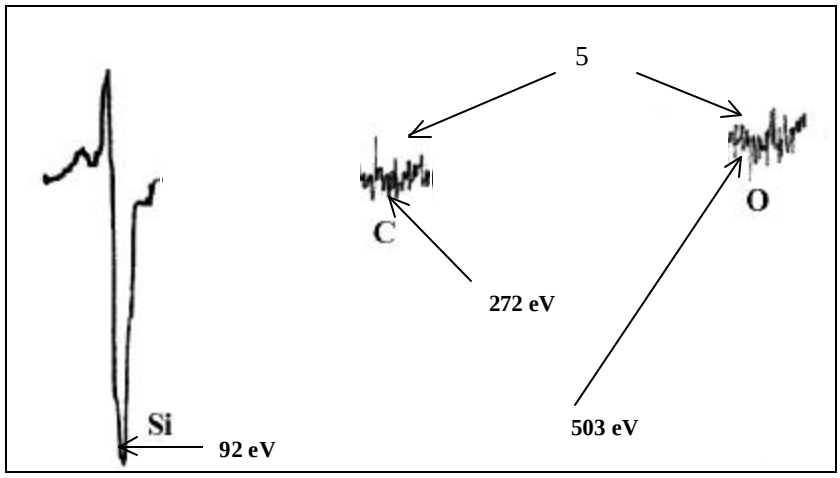

Figure 4.2 Auger spectrum from clean Si(100) 2×1. The Si (92 eV) peak is scaled up by a factor of 5 relative to the rest of the spectrum.

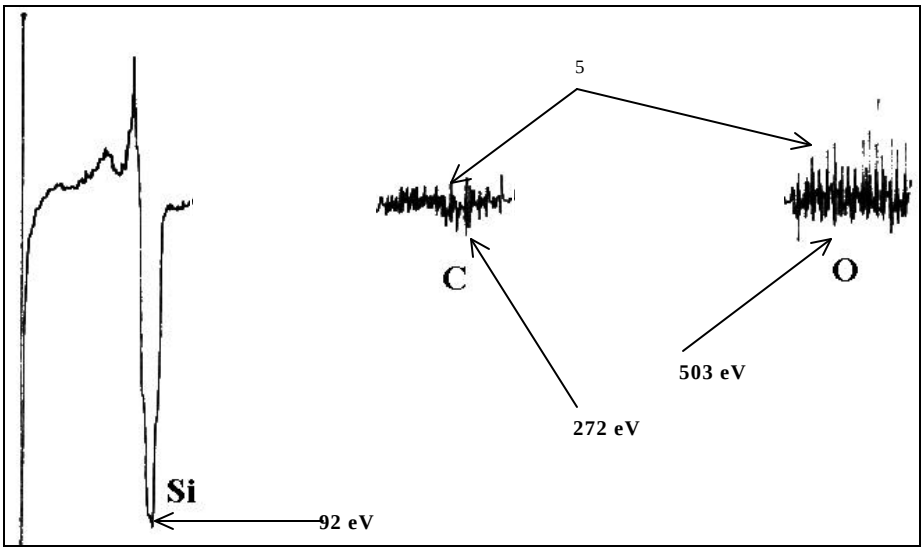

Figure 4.3 AES scan of a clean Si(111) 7×7 surface. The C and O signals are multiplied by a factor of 5 relative to the silicon signal. The C peak is negligible and an O peak is not visible.

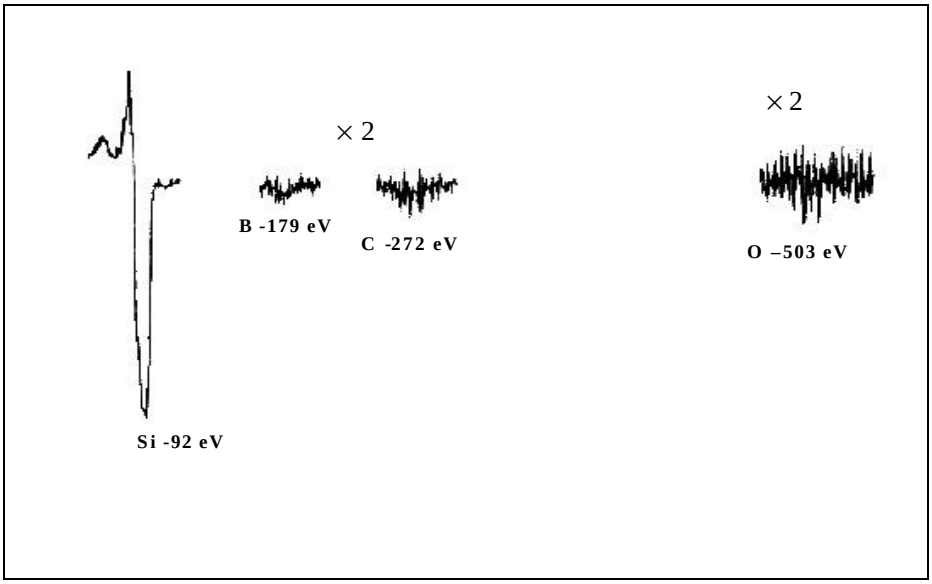

Figure 4.4 AES scan of a Si(111)($\sqrt{3} \times \sqrt{3}$)R30°–B surface. The B, C and O signals are multiplied by a factor of two relative to the Si signal. The C and O peaks are negligible and the B peak is just visible above the noise level.

The value of $\boldsymbol{R_{B-Si}}$ turns out to be about 6% for the clean boron doped surface. While this value may appear to be low, but we should note that the boron is not present on the surface and $\boldsymbol{R_{B-Si}}$ is low due to contributions from other surface and bulk atoms. In fact, it is right in the range of values which are usually taken as indicating a coverage of 1/3 ML in other studies.[1, 2, 3, 4, 5] The oxygen and carbon levels are negligible.

4.1-c Surface structure of the clean Si surfaces:

The surface structure had to be examined for defects and it was necessary to verify if the desired reconstruction had been achieved during sample preparation. LEED images of the clean sample surfaces revealed that the surface reconstruction in each case is indeed the right one. Also the sharp LEED spots observed indicated, that the surface was fairly well-ordered and defect-free. The $\sqrt{3}\times\sqrt{3}$ surface was obtained by first obtaining a clean 7×7 surface which was deposited with boron and annealed.

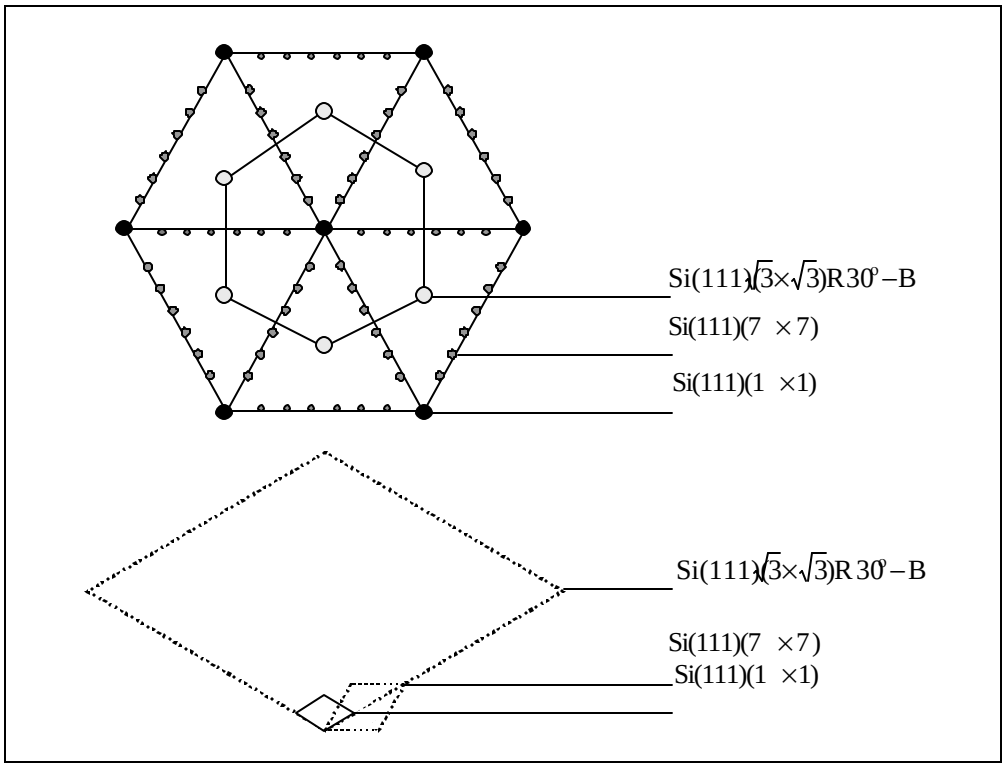

Figure 4.5 a) Superposition of two LEED patterns of Si(111) before and after B doping. The black spots show a 1´1 LEED pattern seen in both cases, the dark grey spots are the main spots corresponding to the 7´7 pattern and the large light grey spots correspond to the pattern which show a 30 degree shift in the axis of symmetry(for the sake of simplicity all spots are not included only those which lie along the principle axes of symmetry) b) The 3 surface lattices superimposed on each other.

We illustrate in Figure 4.5 the difference between the Si(111) 7×7 and the Si(111)($\sqrt{3}\times\sqrt{3}$)R30°–B diffraction patterns obtained before and after boron deposition, by superimposing the two patterns. There is an expected 30° rotation of the axis of symmetry, which verifies the structural transition. For the sake of simplicity all the spots observed especially those of the 7×7 are not shown in Figure 4.4, only the brighter ones or ones which lie along the principle axes of symmetry.

4.1-d Contaminant levels of the cesiated Si surfaces

The contaminant levels of the surfaces increase a bit after Cs deposition. As explained previously, these levels can be determined approximately from the relative size of the Auger peaks of the impurities compared to those of the initial Si peak. To get an idea of the coverage though, the different emission strengths of Auger electrons from different layers have to be taken into account. An estimate of the relative concentrations of the adsorbed elements, is more easily obtained as shown in Table 4-2, Table 4-3, and Table 4-4. It is impossible to completely eliminate contaminants during deposition but by taking appropriate precautions, the contaminants can be kept within acceptable levels.

The carbon Auger peaks, of all our samples (Table 4-2, Table 4-3, and Table 4-4) are barely detectable. The oxygen peak in the most contaminated of the samples studied, corresponded to a coverage of less than 2-3 %. As expected, the oxygen content of the Si(100) 2×1 surface is the highest, since it is the most reactive of all the surfaces studied. The Si(111)($\sqrt{3}\times\sqrt{3}$)R30°–B surface is the most passivated of all the surfaces studied, but shows the same level of contaminants as the Si(100) surface because it is subjected to more intensive processing compared to the other surfaces. The samples corresponding to 5% or higher contamination levels were not used for experiments.

To summarize, even in the worst case which occurred only in a few of the Si(100) surfaces), at least 95 % of the sample surfaces were contaminant free. At such levels, the

contaminants on all the three surfaces should have negligible effect on the RBS measurements reported here.

Figure 4.6 shows an Auger spectrum taken from a cesium-saturated Si(100) 2×1 surface. As expected, since this surface is more reactive than the 7×7 reconstructed surface, it contained somewhat more oxygen than the 7×7 interface. Nevertheless, as shown in Table 4-2, at least 91% of the adsorbed atoms are cesium. The percentages in.

Table 4-2 represents the relative concentrations of the surface adsorbates and should not be confused with absolute coverage of the surface. Subsequent RBS measurements which reveal a Cs coverage of 0.5 ML imply oxygen and carbon coverages of approximately 2.5 % each for this particular sample.

As explained earlier the contaminant levels on the Si(111) surface are found to be lower than that for Si(100). Moreover the fresh sample can be left for longer periods of time without appreciable contamination.

Figure 4.8 and Table 4-4 illustrates the quality of a typical Si(111)($\sqrt{3}\times\sqrt{3}$)R30°–B sample used in the RBS measurements. The impurity atoms make up roughly 4% of the total adatoms(not counting B atoms). Subsequent RBS measurements show that the coverage is less than .5 ML, which means that the absolute concentrations of the impurity atoms are less than 2-3 %. Boron deposition followed by annealing does introduce more impurities into the surface but the contaminant levels are comparable if not better than those of the Si(100) and Si(111) 7×7 surfaces.

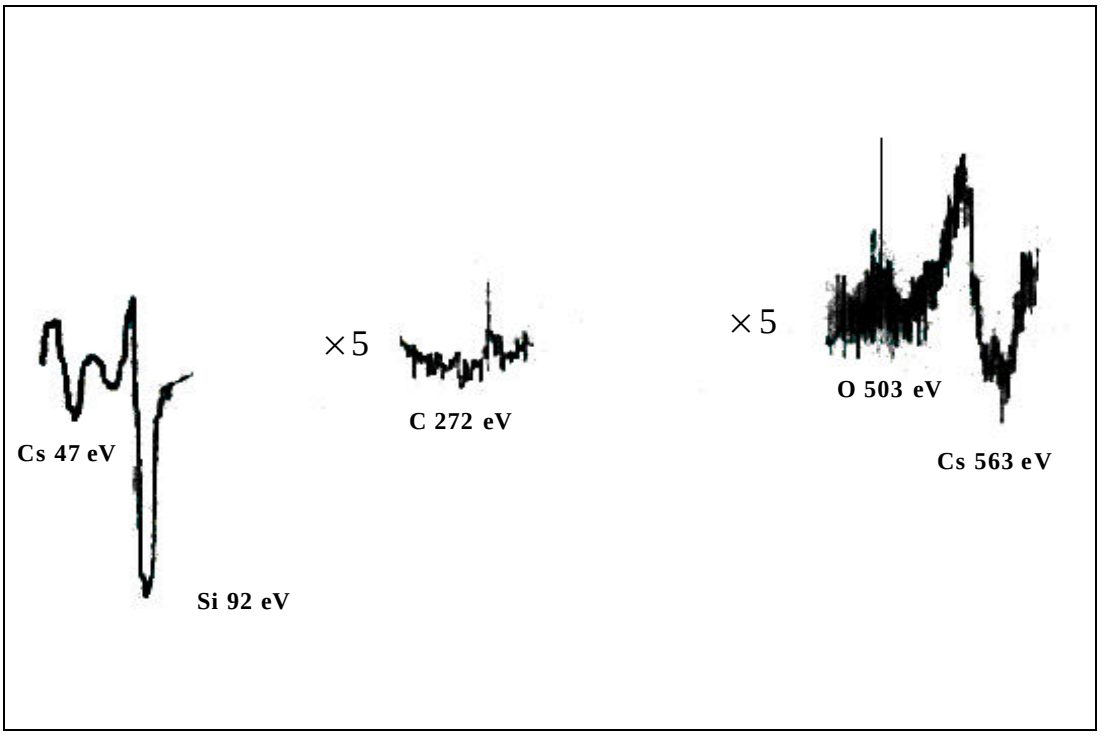

Figure 4.6 Auger spectrum from cesium saturated Si(100) 2×1. Note the low energy Cs (47 eV) and Si (92 eV) peaks are scaled up by a factor of 5 relative to the other peaks. (The thin spikes in the C and O peaks are just noise.)

Table 4-2 Contamination estimates for a saturated Cs/Si(100) 2×1.

Element	Signal Height (mm)	Sensitivity Factor[6]	Relative Atomic Concentration (signal/sensitivity)	Percentage
C	2	0.21	10	5%
O	5	0.52	10	5%
Cs	32	0.17	188	91%

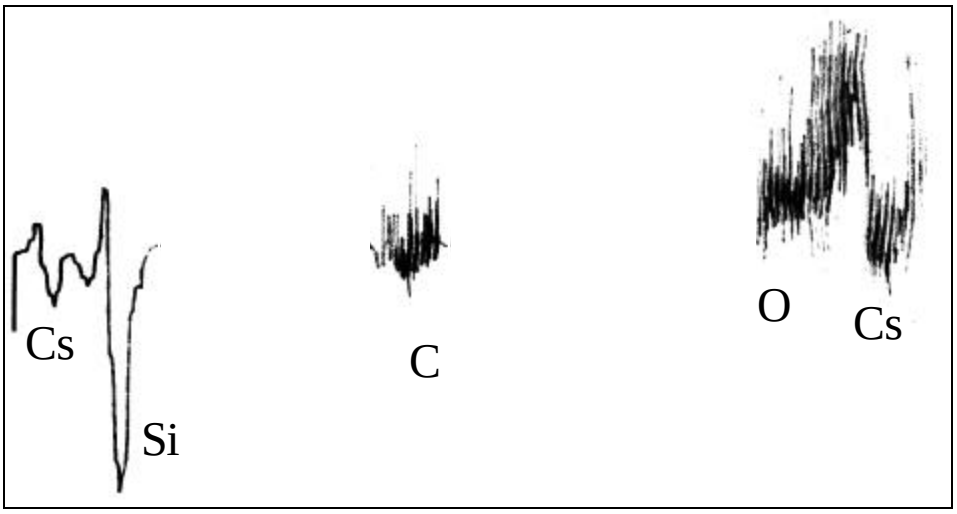

Figure 4.7 Auger spectrum for the cesium saturated Si(111) 7×7 interface. Vertical axis is dN/dE, horizontal axis is energy (same for all following spectra). The low energy Cs (47 eV) and Si (92 eV) peaks are scaled down by a factor of 5 relative to the other peaks. (The tall, thin spikes in the C and O peaks are just noise.)

Table 4-3 Auger intensity comparison of the possible contaminant level of the Cs/Si(111)7×7 interface.

Element	Peak Energy (eV)	Signal Height (mm)	Sensitivity Factor[6]	Relative Atomic Concentration (signal / sensitivity)	Percent
C	271	2	0.21	10	4%
O	503	2	0.52	4	2%
Cs	563	35	0.17	206	94%

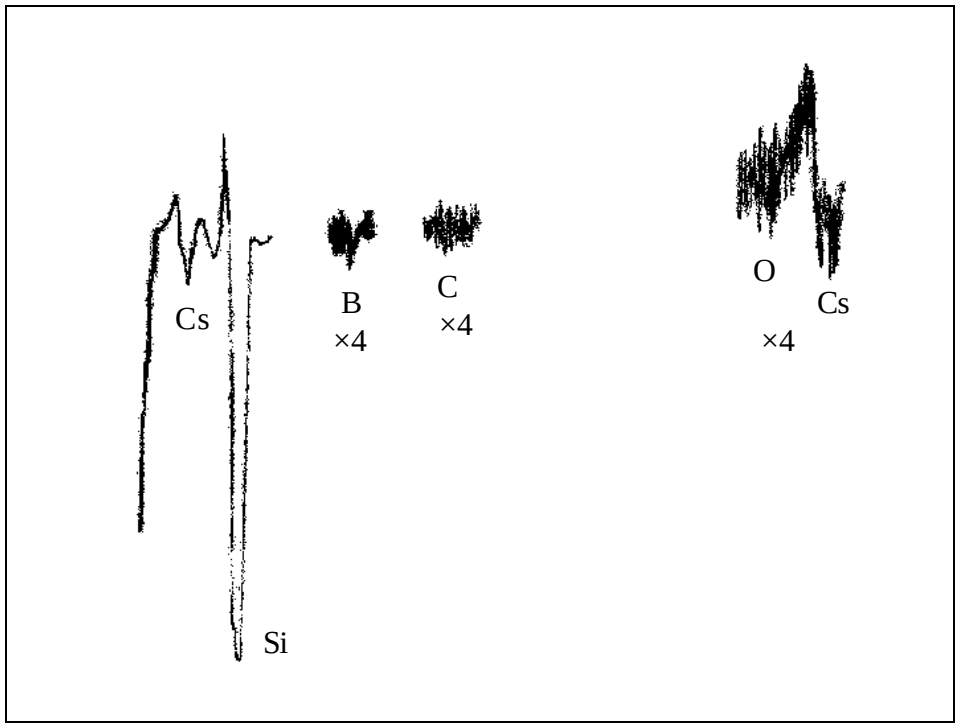

Figure 4.8 Auger spectrum for the cesium saturated Si(111)($\sqrt{3}\times\sqrt{3}$)R30°–B interface. Vertical axis is dN/dE, horizontal axis is energy (same for all following spectra). The low energy Cs (47 eV) and Si (92 eV) peaks are scaled down by a factor of 5 relative to the other peaks. (The tall, thin spikes in the C and O peaks are just noise).

Table 4-4 Auger intensity comparison of the possible contaminant level of the Si(111)($\sqrt{3}\times\sqrt{3}$)R30°–B.

Element	Peak Energy (eV)	Signal Height (inch)	Sensitivity Factor[6]	Relative Atomic Concentration (signal / sensitivity)	Percent
C	271	0	0	0	0%
O	503	.4	0.52	.77	3.5%
Cs	47	.78×4	0.17	18.353	82.7%
B	179	.4	0.13	3.07	13.8%

4.1-e Determination of onset of cesium saturation

Other than examining the purity and structure of the surfaces, it was also necessary to determine the onset of saturation of the surfaces at room temperature. Saturation coverage was determined with the help of the AES uptake curve. As Cs is deposited on to the sample surface, the height of the Cs AES peak grows in relation to the substrate Si signal. After saturation, no more Cs sticks to the surface and the relative and absolute signal strengths of Si and Cs remain the same regardless of further deposition. Thus a good method for the determination of saturation is to study the signal strength of Cs vs that of clean Si, as a function of deposition time.

Saturation is characterized by a cutoff in the Cs/Si auger signal ratio versus deposition time curve as seen in Figure 4.9, Figure 4.10, and Figure 4.11. The cesium deposition rate, keeps varying throughout the life of the doser. Therefore the saturation deposition time needs to be re-calibrated periodically as the doser ages. To ensure saturation during RBS experiments, the deposition times always exceeded the experimentally determined saturation deposition time by a good margin. It was also found that post saturation deposition did not increase contaminant levels or cesium levels by any detectable amount, probably because the saturated surfaces were less reactive. Surfaces with high (greater than 5%) initial levels of contaminants tended to adsorb more cesium even after saturation was reached.

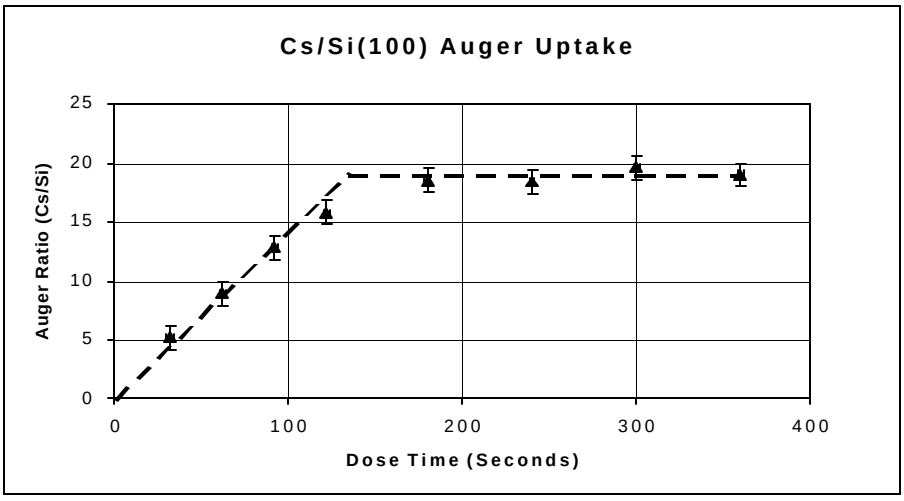

Figure 4.9 Auger uptake curve for Cs on the Si(100) 2×1 surface.

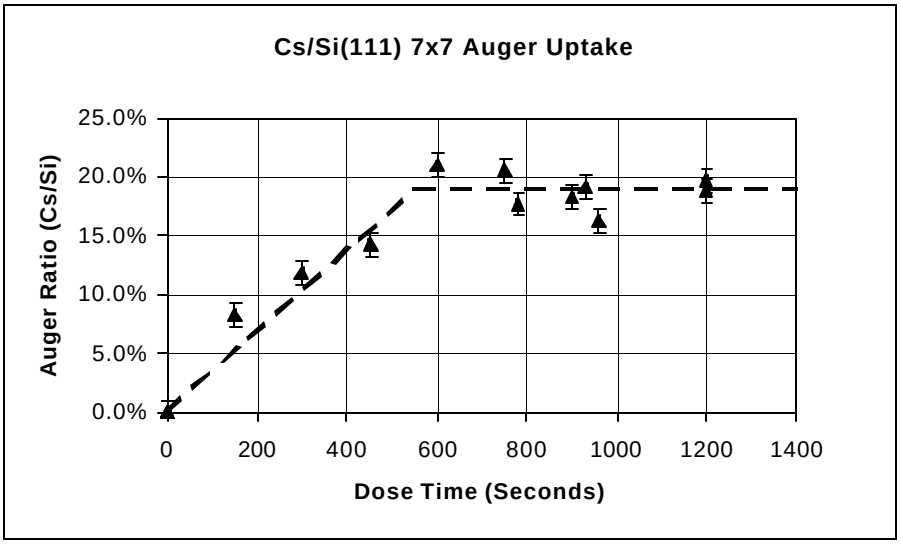

Figure 4.10 Auger uptake curve for Cs on the Si(111) 7×7 surface.

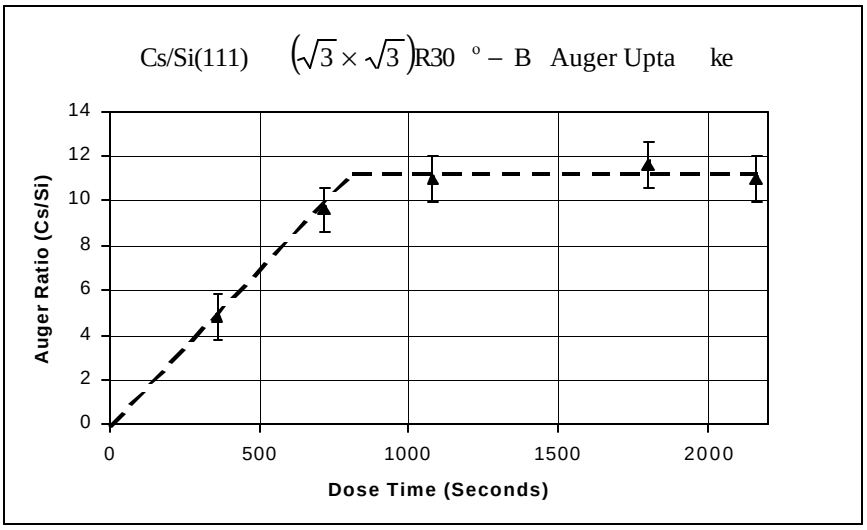

Figure 4.11 Auger uptake of Cs on the Si(111)($\sqrt{3}\times\sqrt{3}$)R30°–B surface.

4.2 RBS of Saturated Cs/Si(100)-2×1

Figure 4.12 shows an RBS spectrum taken from saturated Cs/Si(100) 2×1. A RUMP[7] generated fit is also shown. In agreement with Moore's[8] measurements of multiple scattering events, at lower energies, the simulation drifts below the level of the data. At such low energies, ions, which penetrate a slab of the sample of areal density 1.2×10^{18} atoms/cm^2, are detected at an energy of 180 KeV. At that point on the graph, the (locally averaged) signal is 4% higher than the simulation. This is only one tenth the depth at which Moore's studies report seeing a 5% rise.[8] However, since these data were collected at half the energy Moore collected at, the resulting fourfold increase in the cross section would arguably result in a 16-fold increase in multiple scattering events due to double scattering alone. Thus the discrepancy between the measurement and simulation is reasonably consistent with multiple scattering effects, as observed by Moore.

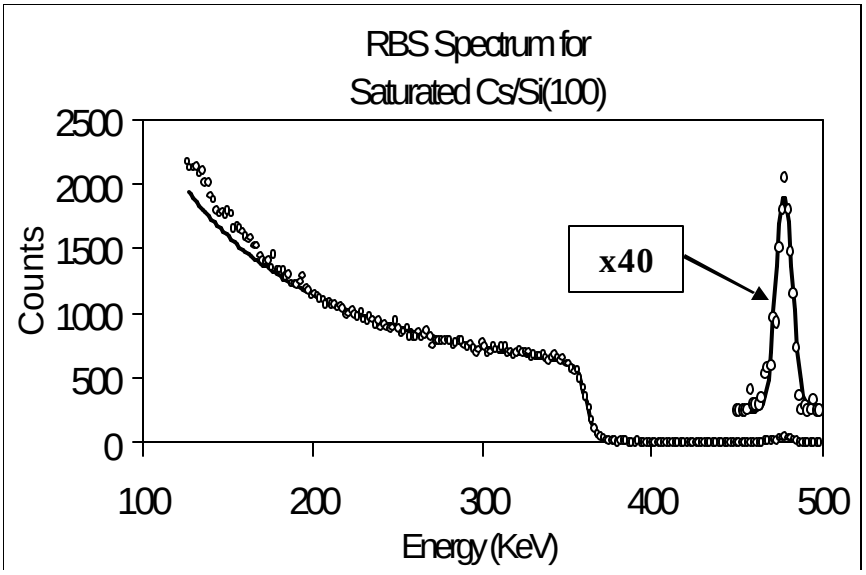

Figure 4.12 RBS spectrum (Q = 50.1°, E = 510 KeV) for saturated Cs/Si(100) 2×1. The experimental data is denoted by circles and the curve is a simulated fit from RUMP.

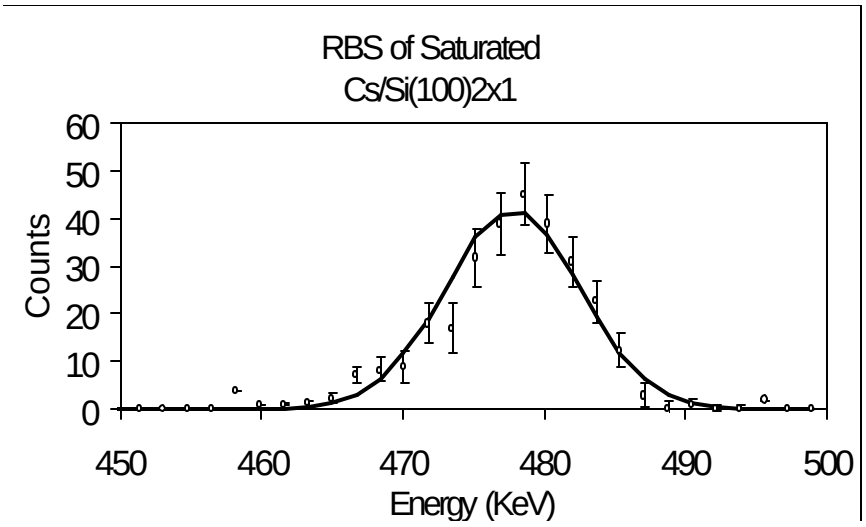

Figure 4.13 The cesium peak from the RBS spectrum of saturated Cs/Si(100) 2×1.

Figure 4.13 shows an enlargement of the cesium peak from Figure 4.12. The general shape of the peak is Gaussian due to the 12 keV energy resolution. The curve in Figure 4.12 and Figure 4.13 is the fit generated by RUMP. The areal density or equivalent thickness of the cesium layer is varied until the area under the simulated and observed peaks is identical (this can generally be done to within 0.1% which is well beyond the experimental precision).In this case, the area under the peaks is 293 counts, which gives a statistical uncertainty $\left(\frac{\sqrt{N}}{N}\right)$= 6%. Combined with the 5% uncertainty from the angular measurements, and the 3% uncertainty from the charge correction factor, this gives a total uncertainty of $\sqrt{3\%^2 + 5\%^2 + 6\%^2} = 8\%$. The RUMP simulation (shown as a solid line) is for 3.2×10^{14} cesium atoms per cm^2, which gives a saturation coverage of 0.47 ± 0.04 ML of cesium.[9]

Table 4-5 Summary of absolute coverage measurements of the saturated Cs/Si(100)-2×1 interface.

Spectrum	Θ	Beam Energy (KeV)	Coverage (Monolayers)	Uncertainty	Weight
1	49.6°	495	0.58	0.07	181.40
2	49.6°	495	0.56	0.05	373.91
3	49.6°	495	0.58	0.05	366.23
4	49.4°	501	0.52	0.07	230.30
5	49.4°	501	0.53	0.05	468.32
6	49.4°	501	0.57	0.05	365.32
7	50.1°	510	0.47	0.04	625.00
Average			**0.54**	**0.02**	

The RBS coverage measurements on the saturated Cs/Si(100) 2×1 interface are summarized in Table 4-5. While one should be concerned over the small amounts of contamination present in the cesium layers, these results should still be considered reliable. Both Soukiassian[10] and our own work have established that contamination of samples tends to increase the surface coverage. It was verified in the current work that poor dosing parameters can introduce high contaminant levels, which can push the cesium coverage up to a maximum of 1.24 ML (determined by converging value of Cs Auger signal strength.). Since the coverage values for the selected samples are much lower than those of samples, which were contaminated while dosing, it is safe to infer that the contaminants did not affect the result significantly. At the same time, a slight contamination level could conceivably explain the observation of a coverage measurement of 0.54 ± 0.02ML instead of exactly 0.50 ML.

4.3 RBS of Saturated Cs/Si(111)(7×7)

Figure 4.14 shows an RBS spectrum from a clean saturated Cs/Si(111) 7×7 sample. A RUMP[7] generated fit is shown. At around 180 KeV beam energy, the number of counts for the experimental data is 8% higher than that of the simulation, and is in qualitative agreement with Moore's studies of multiple scattering effects on silicon.[8] Other than this small accountable discrepancy, the RUMP simulation fits the silicon onset region (corresponding to the near surface layers) nicely.

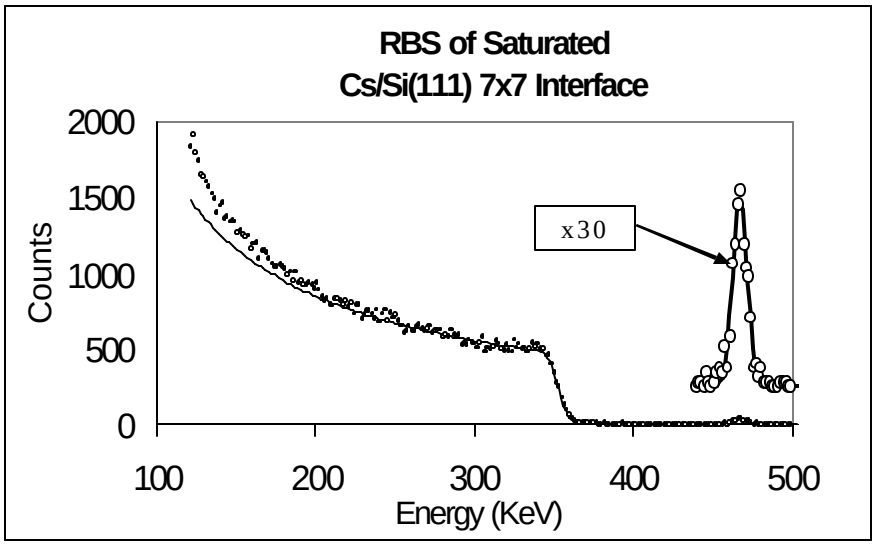

Figure 4.14 RBS Spectrum (Q = 45°, E = 497 KeV) of saturated Cs/Si(111) 7×7 interface with simulation fit of 0.52 ML. Inset is a 30× blowup of the cesium peak

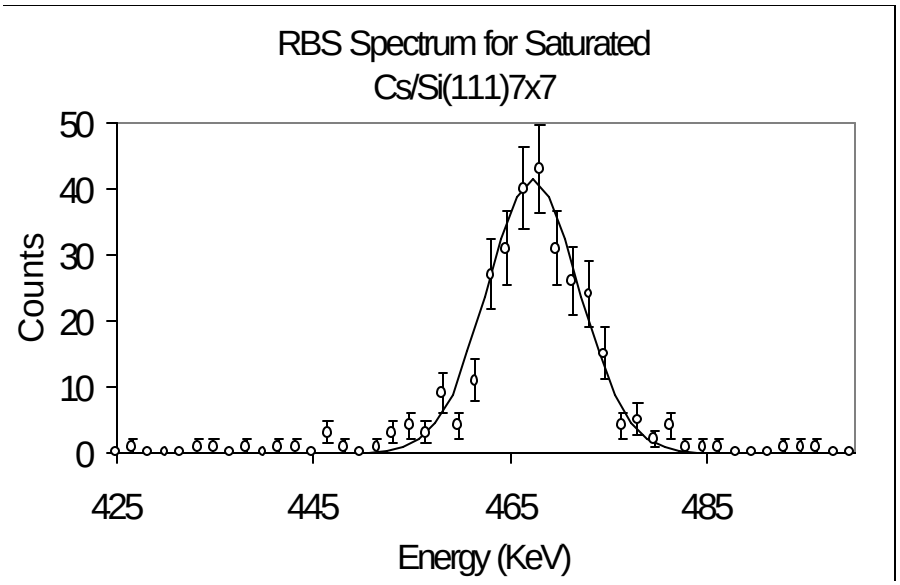

Figure 4.15 Enlarged section of the RBS spectrum of the saturated Cs/Si(111) 7×7 interface showing a RUMP generated fit with an equal area under the peak.

Figure 4.15 shows an enlarged version of the cesium peak shown Figure 4.14 with the statistical error bars included. The area or counts in the simulated Cs curve is 293 and exactly the same as the counts corresponding to Cs peak obtained by experiment. The statistical uncertainty for this number of counts is 6%. Given the 5% uncertainty from angles, and a 3% uncertainty from the current integration, the total uncertainty is $\sqrt{3\%^2 + 5\%^2 + 6\%^2} = 8\%$. This simulation is for 4.08×10^{14} cesium atoms per square centimeter which gives an observed saturation coverage of 0.52 ± 0.04 ML. Table 4-6 below summarizes all the absolute coverage measurements Cs on Si(111) 7×7.

Table 4-6 Summary of absolute coverage measurements for saturation of Cs/Si(111) 7×7.

Spectrum	Θ	Beam Energy (KeV)	Coverage (Monolayers)	Uncertainty (Monolayers)	Weight
1	45°	500	0.45	0.06	269.48
2	45°	500	0.52	0.04	542.82
3	45°	500	0.51	0.04	575.66
4	45°	500	0.51	0.07	202.09
5	45°	500	0.69	0.08	155.57
6	45°	497	0.48	0.09	132.28
7	45°	497	0.49	0.06	306.15
8	45°	497	0.47	0.05	423.11
Average			**0.51**	**0.02**	

4.4 RBS of Saturated Cs/Si(111)($\sqrt{3}\times\sqrt{3}$)R30°–B

Figure 4.16 shows an RBS spectra from a saturated Cs/Si(111)($\sqrt{3}\times\sqrt{3}$)R30°–B sample obtained after a total charge of 3 μC(1 μC =10^{-6} Coulombs) has hit the sample.

Making a comparision with the other spectra of excess counts due to multiple scattering, we find that for scattered ions at 180 keV, the (locally averaged) signal is 3% higher than the simulation, which is within the acceptable range.

The coverage of this sample turns out to be .34 ML. The number of counts under the curve is 202 and the corresponding statistical error is around 7%. Taking into account the errors in angle measurement (3%) and charge integration (3%), the overall error is $\sqrt{3\%^2 + 3\%^2 + 7\%^2} = 8.2\%$.

Figure 4.18 is the RBS spectrum obtained from a sample with a beam dose of 39μC. Multiple scattering effects are minimal at 180 keV the raw data exceeds the simulation by only 2%. The Cs peak is magnified 60× and shown separately in Figure 4.19. The area under the simulated curve and the number of counts in the data corresponding to the Cs peak are 1562. The corresponding statistical error is 2.5%. Combining this with an angular error of 3% and current integration of 3% we get a total error of $\sqrt{3\%^2 + 3\%^2 + 2.5\%^2}$ = 5%. The simulated curve corresponds to an areal density of $.11\times10^{-15}$ atoms/cm^2. Combining this with the error we get a measured coverage of .1405 ± .0035 ML.

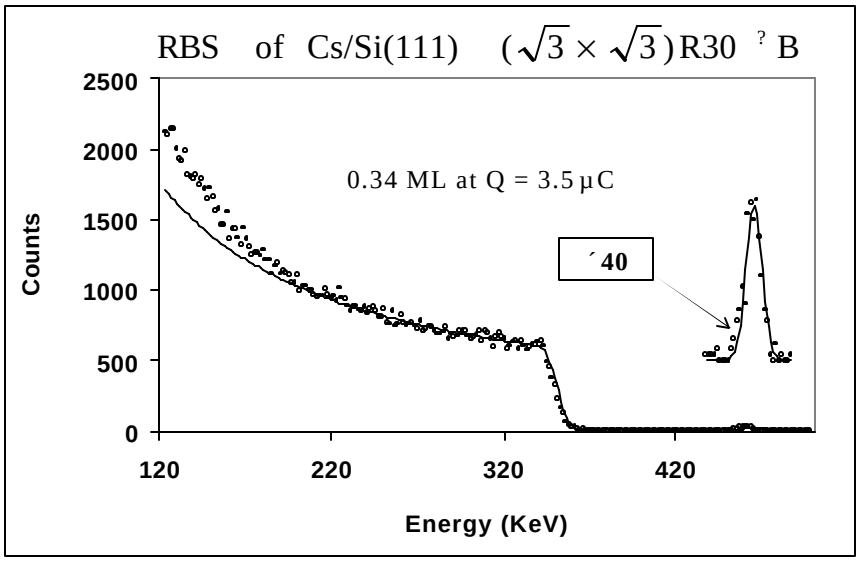

Figure 4.16 RBS Spectrum of the Cs/Si(111)($\sqrt{3} \times \sqrt{3}$)R30°–B interface with Cs region enlarged. RUMP generated fit with equal area under the peak is shown as a curve.

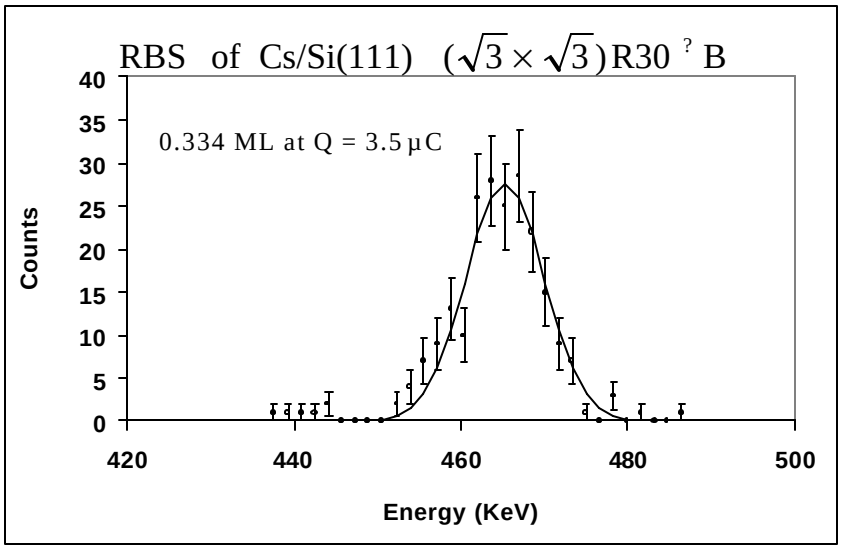

Figure 4.17 Enlarged section of the RBS spectrum of the saturated Cs/Si(111)($\sqrt{3} \times \sqrt{3}$)R30°–B interface showing RUMP generated fit with equal area under the peak.

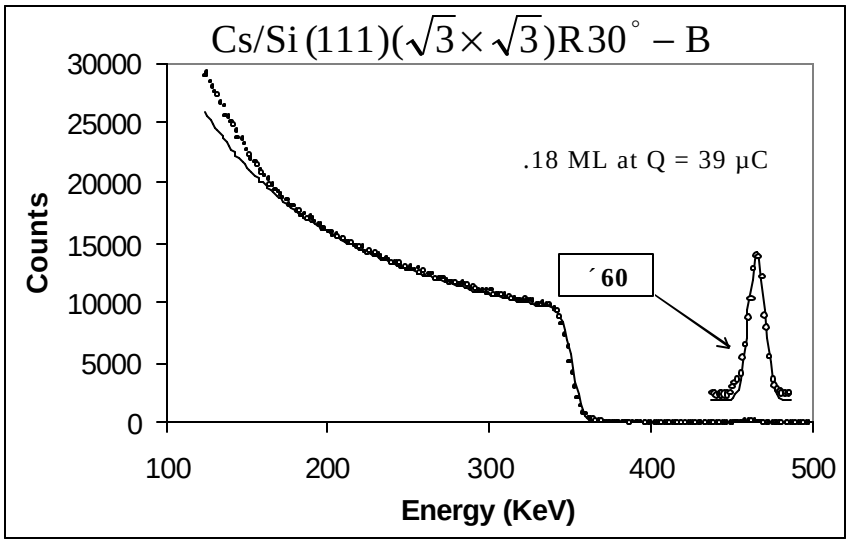

Figure 4.18 RBS Spectrum of Cs/Si(111)($\sqrt{3}$ ´ $\sqrt{3}$)R30°–B interface at a beam dose of 39mC. A simulation fit of 0.18 ML (curve) is shown as a curve. Inset is a 60× blowup of the Cs peak.

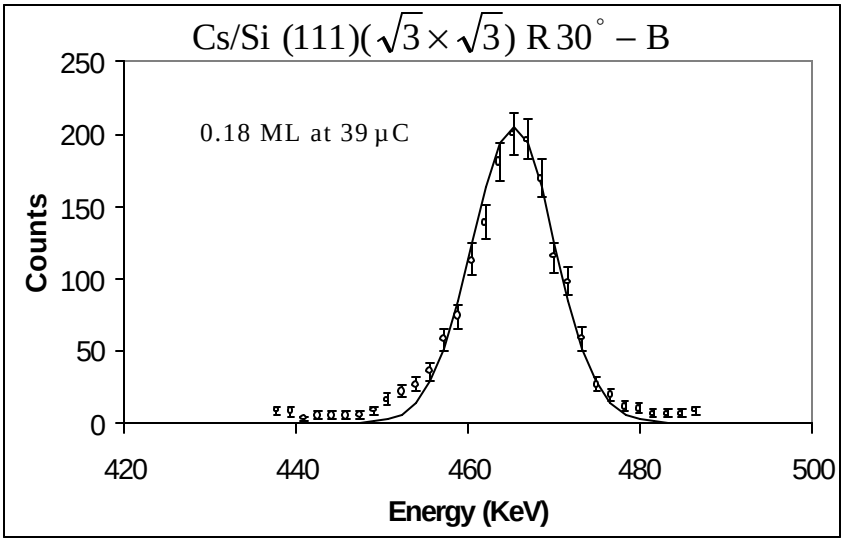

Figure 4.19 Enlarged section of the RBS spectrum of the Cs/Si(111)($\sqrt{3}$ ´ $\sqrt{3}$)R30°–B interface. RUMP generated fit with equal area under the peak is shown as a curve.

The coverage is different for the two samples. The sample with a lower beam dose of 3μC has a coverage of 0.34 ML whereas the sample with a higher beam dose of 39μC has a coverage of 0.18 ML. We should also note that the sample with a higher beam dose has much better statistics than the other one. RBS spectra obtained at different beam doses reveal a decreasing coverage with increasing beam dose (measured in μC). The initial coverage for low beam doses as indicated by the data, is close to the expected theoretical value of 1/3 ML.

Table 4-7 Summary of all experimental data obtained from good Cs/Si(111)($\sqrt{3} \times \sqrt{3}$)R30°–B samples.

Spectrum	Θ	Charge(μC)	Coverage (Monolayers)	Uncertainty (Monolayers)
1	45°	7	.21	0.06
2	40.4°	39	.14	0.04
3	40.4°	45	.14	0.04
4	50°	11	.27	0.07
5	41.6°	3.5	.336	0.08
6	41.6°	7	.303	0.06
7	41.6°	10.5	.3	0.05
8	41.6°	15	.289	
9	43.5°	17	.23	
10	43.5°	23	.217	
11	43.5°	28	.204	

4.5 Ion Beam-induced Desorption of Cesium

Figure 4.20 and Table 4-7 show decreasing coverage with increasing exposure to the ion beam, which measured as cumulative charge, hitting the target. It was verified

that the decay in coverage was occurring due to exposure to the ion beam alone and not due to spontaneous desorption. (The coverage did not diminish during the times when the surface was not exposed to the beam). The initial points are taken with very low exposures and the error margins on them are higher. Nonetheless, we can clearly see that the initial coverage converges to a value that is close to 0.33 ML for small exposures to the beam.

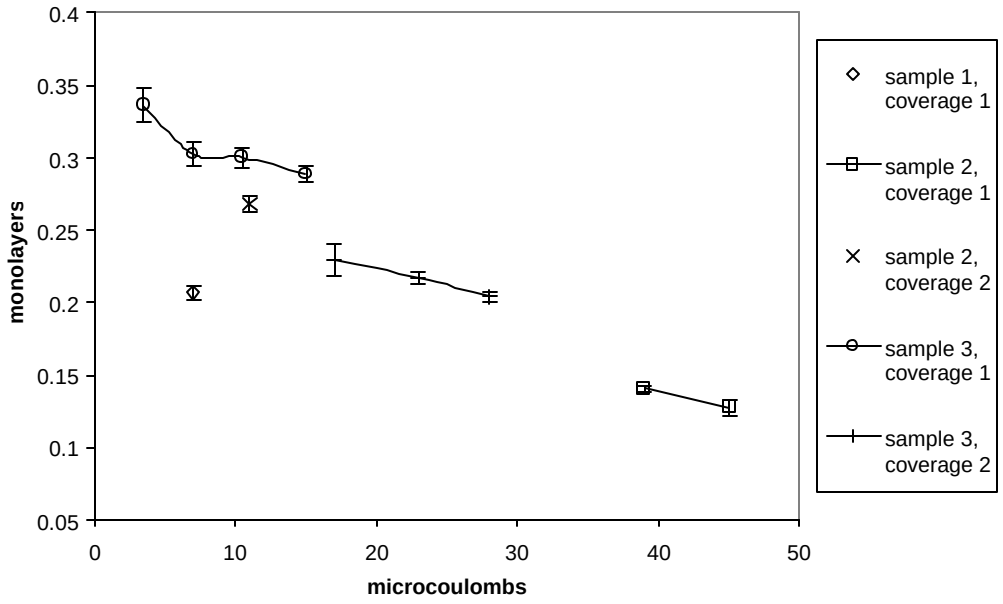

Figure 4.20 Plot of coverage versus ion beam dosage. Dosage is cumulative charge which impinges on the surface. The coverage starts from a maximum of ~1/3rd ML and decreases with increasing exposure to the ion beam particles. The lines connect samples with sequential doses, which have the same geometric parameters for RBS.

The simulation package for analyzing RBS data called RUMP is used to calculate the coverage of the adsorbed cesium layer. It assumes a constant coverage with no

attrition or decay of the cesium layer over time. Our data shows that this is not the case for the Cs/Si(111)($\sqrt{3}\times\sqrt{3}$)R30°–B surface and the helium ion beam induces cesium desorption from the surface. To interpret the RUMP output in this case we need to specifically model RUMP coverage measurement of a desorbing layer.

The coverage measurement depends on the number of recoiling ions detected within a certain energy range. If the coverage remains a constant then for a given amount of charge impinging on a target the same number of counts (recoiling ions) are recorded. As more charge hits the target the number of counts detected go up proportionally. This is expressed by the following equations.

$$C(Q) = \int_0^Q knd\,q \qquad \textbf{Equation 4-1}$$

or

$$C(Q) = knQ \qquad \textbf{Equation 4-2}$$

where *C(Q)* is the number of counts recorded as a function of cumulative charge *Q*. *n* is the areal density of the coverage and *k* depends on many factors like the solid angle of the detector, its exit angle, energy of the incident beam and its orientation with respect to the sample and the atomic number of the nuclei involved in the interaction etc. Equation 3-3 is similar in form to the more detailed relationship as described by the equation for the areal density of a layer in the previous chapter in section 3.1, which can be rewritten as

$$C_i = \frac{Nt_i Q \Omega s_i(E_I, f)}{\cos(f)}$$ **Equation 4-3**

Since we are concerned only with the recoil ions from the topmost layer, it is simpler to express Nt_i as areal density n. The angle and energy dependant part of the function are constants during the course of an experiment or otherwise accounted for by RUMP. For our purposes it can simply be treated as a constant k. With these simplifications, Equation 4-3, assumes the same form as Equation 4-2.

During the experiment counts $C(Q)$ and cumulative charge impinging on the target Q are recorded. The RUMP analysis basically amounts to determination of the areal density n by using the following relationship, which is a simplified form of Equation 3-3.

$$n = \frac{C(Q)}{kQ}$$ **Equation 4-4**

For the Cs/Si(111)($\sqrt{3} \times \sqrt{3}$)R30°–B surface, the areal density of cesium does not remain a constant but it decreases as increasing amounts of charge impinge on the surface. Let us assume that the probability of collision or knocking off, of a cesium atom is a constant and does not depend on the instantaneous coverage and that it takes an average charge of Q_0 to dislodge a Cesium atom present in a unit area. This can also be stated as saying that the probability of 1 unit of charge incident on a unit area, dislodging a cesium atom within it, is $1/Q_0$.

The desorption rate is then proportional to the amount of cesium left on the surface.

$$\frac{dn}{dQ} = -\frac{n}{Q_0} \qquad \textbf{Equation 4-5}$$

solving this equation we get a first order decay rate equation with respect to the charge *q*

$$n = n_0 e^{-Q/Q_0} \qquad \textbf{Equation 4-6}$$

where n_0 is the initial starting value of the coverage before any desorption took place. Combining equations 4-6 and 4-1, we get

$$C(Q) = \int_0^Q k n_0 e^{-Q/Q_0} dq \qquad \textbf{Equation 4-7}$$

or

$$C(Q) = k n_0 Q_0 (1 - e^{-Q/Q_0}) \qquad \textbf{Equation 4-8}$$

As discussed earlier, RUMP analysis yields an apparent coverage given by *C(Q)/kQ* which for the desorbing cesium sample works out to:

$$\frac{C(Q)}{kQ} = \frac{n_0 Q_0}{kQ}(1 - e^{-Q/Q_0}) \qquad \textbf{Equation 4-9}$$

for an actual coverage given by the expression (We should note that it is not possible to obtain an instantaneous value of the coverage, using RUMP simulations.)

$$n = n_0 e^{-Q/Q_0}. \qquad \textbf{Equation 4-10}$$

Figure 4.22 shows a theoretical model of coverage as yielded by RUMP analysis and actual instantaneous coverage for a desorbing layer of material and compares it with measurements and counts for a non-desorbing layer. The shape of the curves, depend on Q_0. The smaller the probability of desorption of a single Cs atom (this means larger values of Q_0), the less steep the apparent desorption curve as analyzed by the simulation (RUMP).

The first-order decay equation derived above does not take into account possible nearest-neighbor interactions of the Cs atoms and may not be expected to fit the data for the whole range of beam dosage from start to finish. Its validity however improves if the fits are for short sequential doses during the course of which the Q_0 or the probability of desorption does not change much. Keeping this in mind, several first-order exponential decay curves adjusted for the RUMP normalization contribution (Equation 4-9) are fitted to the experimental data shown in Figure 4.22.

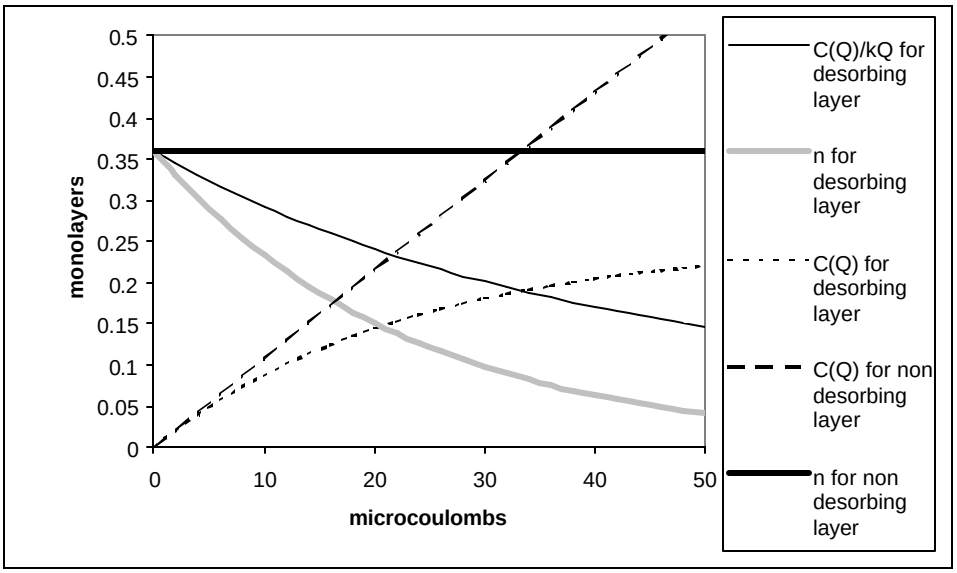

Figure 4.21 A model for apparent and actual coverage as seen by simulations(RUMP), for desorbing Cs adatoms.

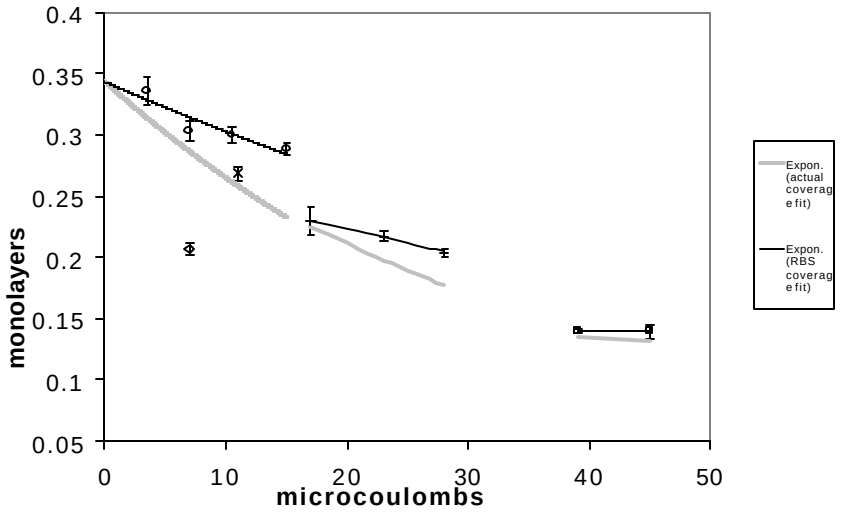

Figure 4.22 A theoretical fit to the apparent coverage of Cs as analyzed by RBS. A constant. coverage independent desorption cross section for the incident ions has been assumed.

Desorption may also depend on the incident angle of the beam as our data also seems to suggest. Since desorption phenomenon was not anticipated before hand, efforts were not made to collect detailed data at different angles or dosages. The incident angles ranged between 40° and 50°, and the data represents the average desorption characteristics for this range of angles. Several fits to experimental data are shown in Figure 4.22. The fits are for the samples, which have undergone sequential beam doses under the same parameters. It is found that the desorption probability (indicated by parameter Q_0) for the different fits is not close to a single constant value but decreases with decreasing coverage. This means that the desorption cannot be modeled strictly as a first order decay.

It is not possible to obtain a true instantaneous coverage measurement from a desorbing layer by RUMP, which integrates counts over time. However we can obtain the saturation coverage value by extrapolating the desorption curve to see what the initial coverage is before the onset of ion beam induced desorption. By extrapolating the theoretical desorption curve for the sample with lowest beam dosage, we obtain a coverage of 0.343 ML (Figure 4.22).

The actual initial coverage can be expected to be a little higher given the fact that the data supports a larger desorption probability at lower coverages. But even then, it would still be sufficiently close to the expected 1/3 ML coverage. We should also consider the fact, that coverages higher than 0.33 ML could be due to contributions from defective regions in the sample surface which do not have sufficient B substitution in the sub-surface layer.

List of References

[1] V.V. Korobstov, V.G. Lifshits, A.V. Zotov, Surf. Sci. 195 466 (1988).

[2] F. Thibaudau, Ph. Dumas, Ph. Mathiez, A. Humbert, D. Satti, F. Salvan, Surf. Sci. 211/222 148 (1989).

[3] S. Bensalah, J.P. Lacharme and C.A. Sebenne, Surf. Sci. 211/222 586 (1989).

[4] J. E.Quinn, Ph.D. dissertation, State University of New York at stoney brook, 1992

[5] T. Tatsumi, I. Hirosawa, T. Niino, H. Hirayama, and J. Mizuki, Appl. Phys. Lett. 57 1395 (1990).

[6] L. E. Davis, N. C. MacDonald, P. W. Palmberg, G. E. Riach, and R. E. Weber. *Handbook of Auger Electron Spectroscopy, Second Edition*, (Physical Electronics Division, Perkin Elmer Corporation, Eden Prairie, Minnesota, 1978).

[7] RUMP - RBS Analysis and Simulation Package [v. 4.00(beta)], (c) 1988-1997 Michael Thompson, Larry Doolittle, (c) 1988-1997 Computer Graphic Service, Ltd. All rights reserved, Revision Level: Version 0.950

[8] J. Moore, Nucl. Instr. and Meth. **174**, 577 (1980).

[9] Where 1 ML is 6.78×1014 atoms/cm2 for Si(100) as discussed in section **2.2** above.

[10] P. Soukiassian, (Private communication).